Magnetotelluric fieldwork adventures in Africa

Magnetotelluric fieldwo

In her RAS Presidential Address for 2005, Kathryn A Whaler discusses how mapping the electrical resistivity of the subsurface can be used to investigate continental rifting, with examples from Africa.

ABSTRACT

The magnetotelluric (MT) method is a way of probing the electrical resistivity (or its inverse, electrical conductivity) distribution of the subsurface. It is based on the principle of electromagnetic induction, in which natural magnetic field sources external to the Earth induce eddy currents within it whose geometry and decay depend on the subsurface resistivity structure. The method is therefore entirely passive, and it can be employed in environmentally sensitive areas. The resistivity of the subsurface depends on its temperature, mineralogy and fluid content, both interstitial and partial melt, and is sensitive to even small amounts of melt and residual fluids and its connectivity. Thus it can be a good discriminant between different rock types, and complements information available from other geophysical methods. Here, I outline the basics of the MT method, indicate how data acquisition, processing and modelling are undertaken, and illustrate the uses of MT to investigate tectonic and structural problems through three case studies from Africa.

The magnetotelluric (MT) method involves recording time series of the magnetic and electric (telluric) fields in orthogonal, horizontal directions often, for convenience, magnetic north–south and east–west, for analysis in the frequency domain. The studies reported here are based primarily on data collected in the audio-frequency range of a few hundred Hz to of order 0.001 Hz, but in some cases extending to longer periods. Above ~1 Hz, the magnetic field source is sferics associated with thunderstorms; at longer periods, solar activity. The magnetic field is trapped in the ionospheric wave guide encircling the Earth and, sufficiently far from the original source (e.g. not adjacent to a thunderstorm), can be approximated as a harmonic, plane wave at infinity. Variations in the induced fields that arise from the different lithologies and structures in the subsurface can be mapped from the measured MT time series.

The challenge in using MT in geophysics is to deduce useful information about Earth structure from these time series. The electric and magnetic signals are related by **Z**, an impedence tensor known as the Earth response (also response function or transfer function), which depends on variations in the resistivity of the area surveyed, reflecting, in turn, the subsurface structure. The MT method involves modelling the data to get the best fit for resistivity in one, two and three dimensions (see "The magnetotelluric method" p2.30). Complications arise because the source field does not take the simple form assumed and lacks energy in key sections of the frequency range, and from the effects of noise.

Data acquisition

Even when the source strength is good, the signals measured in MT are extremely small; thus the equipment must be very sensitive and the signals are amplified considerably, making them vulnerable to noise. The most significant noise sources are energy at mains frequency and its harmonics, cultural noise from the movement of vehicles, people and animals, and wind. Therefore equipment must be deployed in quiet areas – both electromagnetically, so keeping well away from power lines and buildings with electrical power (be it generator or mains supplied), and vibrationally, avoiding trees or dense vegetation, and roads. The magnetic sensors are usually buried to reduce wind noise, but this does not reduce wind-caused tree-root vibration. Away from the main population centres in Africa, it is usually easy to avoid electromagnetic and vehicle noise, but vegetation cover can cause problems.

The electric field, **E**, is deduced from the voltage between pairs of electrodes; separations of 30–100 m are typical. At higher frequencies in non-arid conditions, metal electrodes are adequate, but non-polarizing porous pot type electrodes are used for longer periods and where dry soil conditions would make it difficult to make good electrical contact with the ground. Lead – lead chloride or silver – silver chloride electrodes are stable and maintenance-free over long periods. At high frequencies, the magnetic field, **H**, is monitored by induction coils consisting of many turns of fine wire on a metal core. At longer periods, fluxgate magnetometers are more suitable, although broadband coils are now available for periods of up to several thousand seconds.

I have used equipment loaned from the Natural Environment Research Council's Geophysical Equipment Facility (formerly Geophysical Equipment Pool): SPAM (Short Period Automatic Magnetotelluric) Mk II or III for shorter period data acquisition (Ritter *et al.* 1998), incorporating sampling over a number of frequency bands at different rates, real-time data processing and quality control (though post-processing was also undertaken), and long-period systems based on EDA fluxgate magnetometers, sampling at 20 s. SPAM III incorporates multiple band simultaneous recording using parallel computing methods and, latterly, GPS-based timing to an accuracy of ±2 μs, allowing for remote reference processing (described in "The magnetotelluric method", page 2.30). Typically, SPAM is deployed at sites for a day, and long-period systems for about a month.

Modelling

A variety of modelling algorithms, both forward and inverse, have been developed to treat the problem of inferring resistivity structure from MT data. The inverse problem is highly non-unique and nonlinear, which causes difficulties of stability and computational effort. The non-uniqueness means models are usually subject to sensitivity analysis, whereby the robustness of their features is tested by determining whether they are required by the data. Parker (1980) developed an important existence algorithm for the 1-D case. He showed that the best-fitting model is a series of Dirac delta functions in conductivity, separated by insulating layers, referred to as a D^+ model. The number, conductance and depth of the delta functions are determined by the data. The existence or otherwise of a 1-D model is then determined by the misfit to the D^+ model. D^+ was developed for modelling the complex admittance ($E/i\omega H$, where ω is frequency); subsequently, Parker and Booker (1996) developed the equivalent algorithm, known as ρ^+, for apparent resistivity and phase

rk adventures in Africa

data (see "The magnetotelluric method", page 2.30). At the opposite extreme from the extremely "spiky", non-physical D^+ and ρ^+ models, most interpretable models are produced by seeking the spatially smoothest, or regularized, model fitting the data, a technique first introduced in the 1-D case by Constable *et al.* (1987) and known as Occam modelling. Thus the objective function minimized consists of a term measuring the goodness-of-fit and a term measuring model smoothness, with a free parameter determining the relative importance assigned to the two. The method is iterative, so requires a starting model; typically, this will be a uniform half-space of specified resistivity. The models are over-parameterized, allowing a good fit to the data, and the smoothness constraint minimizes the amount of structure in the model. We then know that the real Earth has at least as much structure as the Occam model. "Smoothness" is usually characterized by a two-norm measure of the gradient or second (spatial) derivative of the model (approximated by first or second differences).

There are various implementations of regularized modelling in two and three dimensions. Two-dimensional Occam (de Groot-Hedlin and Constable 1990) and rapid relaxation inversion, or RRI (Smith and Booker 1991) are the most widely used 2-D algorithms. Over the years, guidelines have been developed for efficient computational implementation, including optimal gridding of the subsurface, and how to incorporate the data. For instance, joint inversion of equally weighted TE and TM mode data (defined in "The magnetotelluric method" page 2.30) from a uniform half-space model tends to give a model dominated by structure derived from the TM mode response (e.g. Livelybrooks *et al.* 1993). These iterative methods require predictions of the data by the current model as part of the computational process, for which efficient algorithms have been developed using both finite difference (e.g. Swift 1967, Brewitt-Taylor and Weaver 1976) and finite element (e.g. Wannamaker *et al.* 1987) techniques.

In the 3-D case, Maxwell's equations do not separate into independent modes, and all four elements of the impedance tensor must be included in modelling. The computational effort is therefore much greater, and only recently has 3-D inversion become routinely practical. Hautot *et al.* (2000) developed a regularized 3-D inversion algorithm, based on the forward mod-

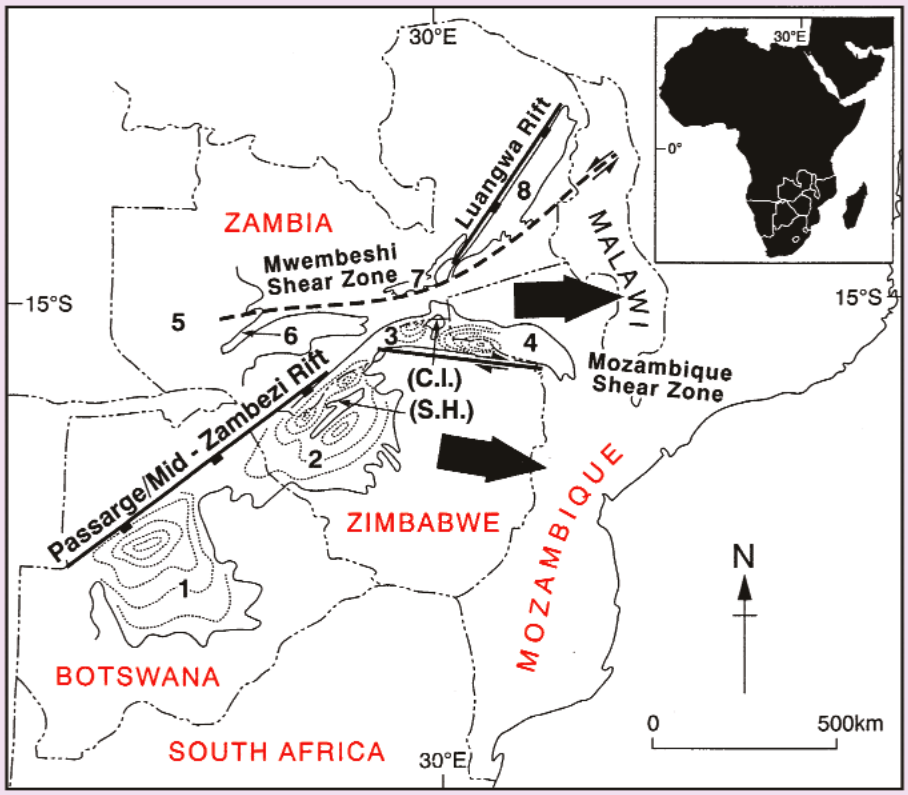

1: Karoo sedimentary basins within the mobile belts of southern Africa. Basins 1–4 lie within the Damara orogenic belt, which extends west of the map area into Namibia, and 3 and 4 are the basins studied here. The contours indicate approximate basement. Basins are: 1 Passarge, 2 Mid-Zambezi, 3 Mana Pools, 4 Lower Zambezi, 5 Western Zambian, 6 Kafue, 7 Launo, 8 Luangwa. The Sijarira horst (S.H.) separates sub-basins within the Mid-Zambezi basin, and the Chewore Inlier (C.I.) separates the Mana Pools and Lower Zambezi basins. After Orpen *et al.* (1989).

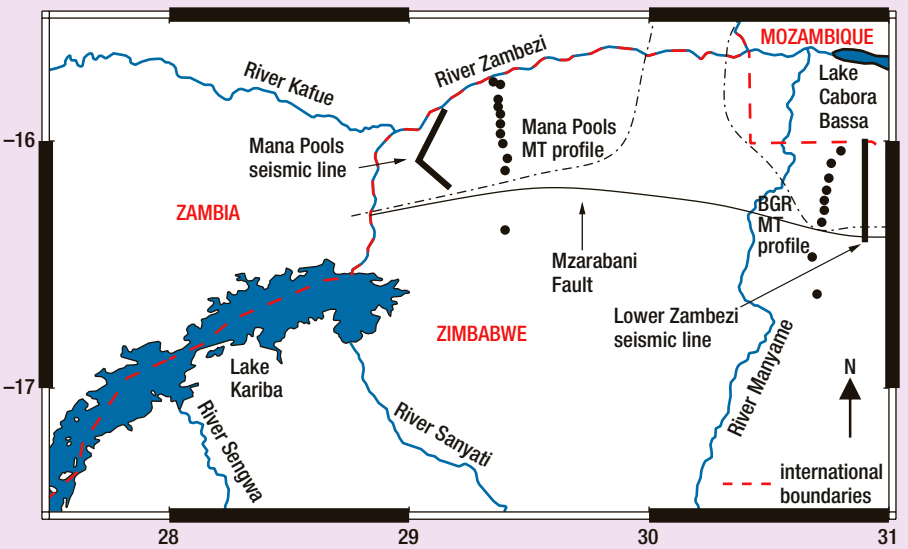

2: Relative locations of the Mana Pools and Lower Zambezi MT and reflection seismic profiles. Dot-dash lines mark the approximate basin boundaries. Dashed lines mark international borders.

The magnetotelluric method

The theory behind electromagnetic (EM) induction methods, including MT, is based on (non-relativistic) Maxwell's equations, assuming that no dielectric or magnetic material is present, and that permittivity and permeability take their free-space values (independent of frequency). Assuming harmonic time dependence for both the magnetic field **H** and electric field **E**, and transforming into the frequency domain, both **H** and **E** satisfy Helmholtz equations $\nabla^2\mathbf{H}-\gamma^2\mathbf{H}=0$ and $\nabla^2\mathbf{E}-\gamma^2\mathbf{E}=0$ where $\gamma^2=i\omega\sigma\mu$, with ω angular frequency, σ electrical conductivity and μ permeability (neglecting displacement currents, which are generally much smaller than conduction currents at the frequencies employed in MT [Telford *et al.* 1990]). These are diffusion (rather than wave) equations, which indicate one of the limiting factors of the MT method – its inherent lack of resolution. Fields are attenuated during propagation and the field strength is large enough to measure only up to some penetration depth; the diffusive nature of the EM signals smoothes out Earth structure (in both the vertical and lateral directions).

The 1-D solution to these equations can be shown to have an electric field varying as $E_x=E_0e^{i\omega t}e^{-\gamma z}$ with x in a horizontal direction and z positive downwards. E_0 is the incident electric field at the Earth's surface. This induces an orthogonal horizontal magnetic field $H_y=H_0e^{i(\omega t-\phi)}e^{-\gamma z}$. H_y lags behind E_x with a phase difference ϕ between the two fields.

An EM field will be reduced in amplitude by a factor $1/e$ at a distance δ within the Earth, known as the skin depth, given by

$$\delta=\sqrt{\frac{2}{\omega\mu\sigma}}=503\sqrt{\frac{1}{f\sigma}}$$

where f is the frequency in Hz (e.g. Vozoff 1972). Thus the MT penetration depth depends on both the period of the signal being measured and the conductivity of the medium. The longer the period measured or the lower the conductivity of the medium, the deeper the EM fields penetrate. The MT impedance Z is defined as the ratio

$$Z=\frac{E_x}{H_y}=\frac{E_0}{H_0}e^{i\varphi} \qquad (1)$$

Hence

$$Z=\sqrt{\frac{\omega\mu}{\sigma}}\,\frac{1+i}{2} \qquad (2)$$

Thus in a homogeneous Earth the complex impedance Z is independent of frequency; its magnitude determines the conductivity, and the phase difference ϕ is 45°.

In a 2-D Earth, Maxwell's equations decouple into two sets of equations. One set, known as the E-polarization or transverse electric (TE) mode, relates the field components E_x, H_y and H_z observed when E_x is parallel to the structure and in the direction of constant conductivity, called the geoelectrical strike direction. The other set, the H-polarization or transverse magnetic (TM) mode, relates H_x, E_y and E_z when the currents are perpendicular to geoelectrical strike. The impedances for the two modes are different because conductivity is no longer homogeneous.

In general, the horizontal electric and magnetic field ratios define an impedance tensor, **Z**, satisfying

$$\mathbf{E}=\mathbf{ZH} \qquad (3)$$

or

$$\begin{pmatrix}E_x\\E_y\end{pmatrix}=\begin{pmatrix}Z_{xx}\,Z_{xy}\\Z_{yx}\,Z_{zz}\end{pmatrix}\begin{pmatrix}H_x\\H_y\end{pmatrix}$$

Z is also known as the Earth response, response function, or transfer function. It is far from straightforward to obtain good estimates of the impedance tensor elements from measured time series of the electric and magnetic fields, for several reasons. The source field is not the assumed harmonic plane wave at infinity, and suffers from lack of energy, particularly in the so-called "dead band" at around 1–10 s period. Even with careful data acquisition, the data are contaminated (biased) by non-zero mean, non-Gaussian noise. Thus robust methods of transfer function estimation are employed (e.g. Egbert and Booker 1986, Chave and Thomson 1989). In addition, if two or more sites record synchronously, their transfer functions can be estimated by a cross-power spectral method known as remote referencing (Gamble *et al.* 1979), by assuming the signal is correlated between the two sites but the noise is not. Remote reference estimation can be used to obtain usable transfer functions even when the data suffer severe noise contamination in some circumstances.

Comparing (1) and (3) it can be seen that, in a 1-D Earth, **Z** takes the form

$$\mathbf{Z}_{1D}=\begin{pmatrix}0&Z\\-Z&0\end{pmatrix}$$

where Z is given by (2) (e.g. Zhang *et al.* 1987). The sign change indicates that the phase is in the third quadrant for the equation relating E_y to H_x. As already noted, the equations relating the electric and magnetic fields decouple for a 2-D

elling difference equations method of Mackie *et al.* (1993). Further complications can occur if conductivity is anisotropic, and distinguishing between 3-D and anisotropic subsurface conductivity distributions is particularly difficult. Most treatments have been concerned with at most 2-D anisotropic media (e.g. Pek and Verner 1997).

The electromagnetic fields satisfy a diffusion equation, rather than the wave equation appropriate for seismology. This means the boundary conditions for 2- or 3-D modelling have to be applied carefully, and that structures some distance from a site influence the MT data measured. Thus the area or volume over which a 2- or 3-D model is parameterized must be significantly larger than that encompassed by the sites. This adds further to the computational burden.

Case studies

Here, I present examples from three (previously published) MT case studies from Africa. The first is from the Zambezi Valley in northern Zimbabwe, where the aim was to infer sedimentary thickness in the Karoo basins, and establish whether an extremely good subsurface conductor running through much of the Damara orogenic belt in southern Africa was continuous. The second is a 3-D investigation of the sedimentary history of the Baringo-Bogoria region of the Kenyan rift. Finally, the power of a multidisciplinary study is demonstrated in the interpretation of a profile across the northern main Ethiopian rift.

Zambezi Valley, northern Zimbabwe

A simplistic description of the African continent divides it into stable cratonic blocks and mobile belts. Rifting between the late Permian and early Tertiary led to the formation of several Karoo basins within the mobile belt terranes, whose tectonic and structural development is described by Orpen *et al.* (1989). A number of previous studies (e.g. Haak and Hutton 1986 and references therein, Losecke *et al.* 1988) had established that there is an extremely good electrical conductor beneath the Damara orogenic belt in Namibia, Botswana, Zambia and parts of Zimbabwe (figure 1). The Mana Pools portion of the mobile belt in the Zambezi Valley of northern Zimbabwe was a "missing link", since its electrical structure had not been probed before 1987, when our study began. In addition, aeromagnetic and gravity data had been used to investigate the thickness of sediments in both the Mana Pools and Lower Zambezi (sometimes referred to as Cabora Bassa) basins in the Zambezi valley, but the interpretation of the aeromagnetic data was ambiguous (Bosum and Geipel 1988). Although the original exploration aim of investigating the basins was uranium prospecting, there was also interest in their hydrocarbon potential, and a reflection seismic survey was shot (Hiller and Buttkus 1996). Unfortunately, both basins straddle international boundaries (with Zambia and Mozam-

Earth, with the electric field component E_x only inducing an orthogonal magnetic field H_y, and similarly E_y inducing the orthogonal H_x. Thus the 2-D impedance tensor also has only non-zero off-diagonal elements, but now their magnitudes will differ:

$$\mathbf{Z}_{2D} = \begin{pmatrix} 0 & Z_{xy} \\ Z_{yx} & 0 \end{pmatrix} \quad (4)$$

(e.g. Zhang *et al.* 1987). In the general, 3-D case, all elements of the impedance tensor are non-zero. This is also true for a 2-D Earth if the geoelectrical strike direction does not coincide with one of the horizontal co-ordinate axes but, in this case, the impedance tensor can be rotated into horizontal co-ordinates parallel and perpendicular to strike: $\mathbf{Z}'(\theta) = \mathbf{R}(\theta)\mathbf{Z}\mathbf{R}^T(\theta)$ where $\mathbf{R}$ is the rotation matrix

$$\mathbf{R} = \begin{pmatrix} \cos\theta & \sin\theta \\ -\sin\theta & \cos\theta \end{pmatrix}$$

and θ is the anticlockwise angle of rotation (e.g. Swift 1967). In this new reference frame, the diagonal elements of $\mathbf{Z}'$ vanish. The components of the impedance tensor can be expressed in terms of a quantity with units of resistivity, based on the amplitude, and phase:

$$\rho_{aij}(\omega) = \frac{1}{\mu\omega \left| Z_{ij}(\omega) \right|^2} \quad (5)$$

$$\varphi_{ij}(\omega) = \arctan \frac{\mathrm{Im}\{Z_{ij}(\omega)\}}{\mathrm{Re}\{Z_{ij}(\omega)\}} \quad (6)$$

ρ_a is known as the apparent resistivity, and is the actual resistivity of a uniform Earth (as can be deduced from equation [2]). MT data are often presented as apparent resistivity and phase as a function of period, as plots from individual stations, or, for data along (or projected onto) a profile, as data pseudo-sections.

In general, there is no rotation angle θ for which the diagonal elements of the impedance tensor vanish, even if the data have been collected over an approximately 2-D region. Most algorithms seek the rotation angle for which they are a minimum. The extent to which any minimum is well-defined indicates how good the 2-D approximation is. For a 1-D Earth, the diagonal elements vanish for all rotation angles, and for a 3-D Earth, for no rotation angle. However, this angle can be a function of period, indicating a change in strike direction with depth, and can change from station to station. For the 2-D approximation to be realistic, there should be a well-defined rotation angle for which the diagonal elements are small that is approximately constant for the survey and does not vary significantly with period. In such circumstances, the data can be rotated into the new co-ordinate system, and the diagonal impedance tensor elements ignored. It is also necessary to determine which of the two off-diagonal impedance tensor components corresponds to the TE mode and which to the TM mode (there is a 90° ambiguity in θ). There are several rotational invariants that can be calculated from impedance tensor components (see e.g. Simpson and Bahr 2005 for details). Quantities such as the determinant or Berdichevsky average are useful for 1-D modelling, since they are thought to be less affected by noise and distortion. Others are useful indicators of the (minimum) dimension of Earth structure.

The 2-D approximation most often fails due to local 3-D distortion, frequently galvanic, by small-scale, near-surface inhomogeneities. This can be tested for and the distortion removed (as far as possible) to leave the signal resulting from the dominant 2-D structure. Several methods have been proposed to undertake this tensor decomposition and assessment. A commonly applied technique is that of Groom and Bailey (1989), who resolved the distortion of an underlying 2-D structure into parts describing twist, shear and anisotropy which have a geophysical interpretation. Bahr (1991) showed how the data can be divided up into classes defined by the degree of distortion, which indicate the type of decomposition (based on an earlier parameterization of the distortion tensor [Bahr 1988]) and subsequent modelling that is appropriate. Bahr (1991), Smith (1995) and Balasis *et al.* (1997) showed that Groom and Bailey's (1989) decomposition of the distortion tensor is equivalent to Bahr's (1988) parameterization.

In the field, galvanic distortion may be revealed by static shift, a DC offset between the apparent resistivity curves at the shortest periods in the two orthogonal directions. Correcting for static shift, i.e. moving one or both of the curves up or down such that they coincide at short periods, can be achieved using independent data that provide a model of the shallow resistivity structure. Most commonly, this information is obtained from DC resistivity sounding or the transient electromagnetic method (TEM) (e.g. Meju 1996). Alternatively, it is possible to solve for a static shift term in conjunction with inversions for subsurface structure. Another possibility is to neglect the apparent resistivity data and model only the phase information, which is unaffected by static shift.

bique), and the geophysical information is confined to Zimbabwe.

We collected audio-frequency MT data at 11 sites along a profile through the Zimbabwe portion of the basin (which comprises most of it) and onto the Zimbabwe craton to the south; at five sites, longer period data were also collected (figure 2). Robust response function estimation produced acceptable values at most sites, although the electric and magnetic field time series were insufficiently coherent at longer audio-frequency MT periods and the shortest periods obtainable from the long-period data for usable data to be obtained. This left a gap between periods of about 10 and 100 s, so the ρ^+ modelling technique was used to check that the data were mutually consistent. Both Groom-Bailey and Bahr distortion analyses were undertaken, which indicated that the data were reasonably consistent with a 2-D structure approximation (Bailey 1998), with a geoelectrical strike direction of approximately 80° appropriate for most periods at most sites.

Two-dimensional RRI of the data was undertaken (Bailey 1998, Bailey *et al.* 2000a). The optimum model has a good conductor to depths of between 5 and 10 km beneath the valley, thinning and becoming less conductive to the south, a resistor at the surface beneath the Zimbabwe craton, and a relatively uniform basement resistivity beneath both the valley and craton. The shape of the good conductor beneath the valley corresponds reasonably well with the basin structure inferred from the seismic reflection survey shot slightly to the west (Hiller and Buttkus 1996, see figure 2), which also indicated that the southern boundary fault of the basin is steeply dipping to the north and reaches a depth of at least 7 km. We expected a similar resistivity contrast at the northern escarpment in Zambia about 10 km north of our most northerly site. With the bounding faults included as vertical discontinuities (across which the smoothness constraint was not applied), the fit to the data at stations close to the basin edges was significantly improved, both numerically and in terms of matching the shape and trend of the data curves. The resistivity of the material to the north of the northerly bounding fault was set to 2000 Ωm (higher than that inferred for the Zimbabwe craton to the south); increasing it improved the fit to the TE mode apparent resistivity, but the fit to the phase deteriorated, and vice versa when the resistivity was decreased. Further improvement was obtained when only the phase data from the most southerly site on the craton were included in the inversion; there was a suggestion that the apparent resistivity data were static shifted. The structure of the final geoelectric section (figure 3) is in good agreement with the seismic reflection model (Hiller and Buttkus 1996) and supports Orpen *et al.*'s (1989) interpretation of the basin as a half-graben with an asymmetric cross-section and a depocentre offset to the northwest. The mater-

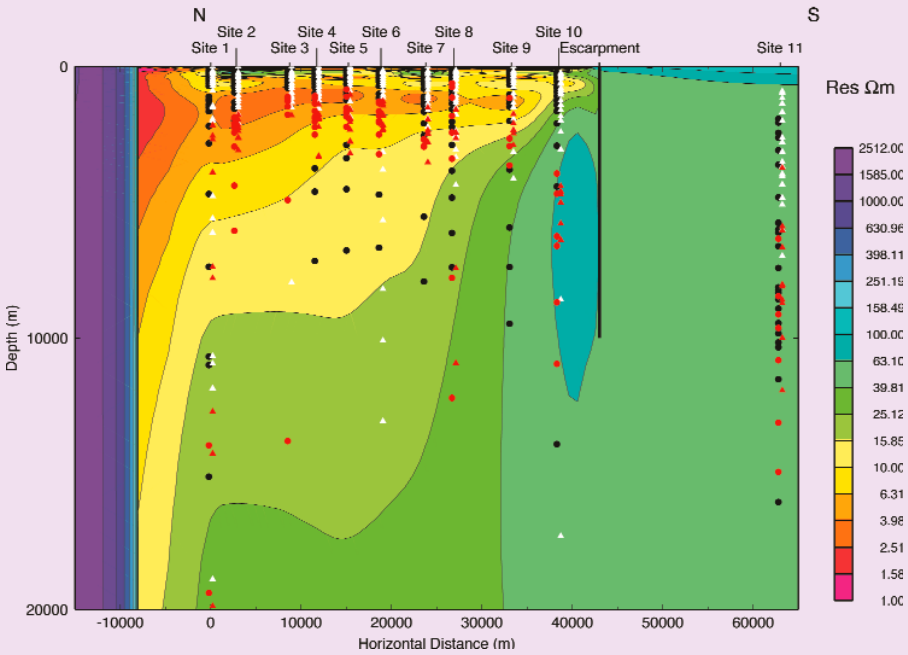

3: The resistivity structure of the Mana Pools basin, with vertical breaks in structure allowed across the locations of the northern and southern escarpment faults. Triangles and circles represent the TM and TE polarization data points plotted at one skin depth respectively, indicating the penetration depth of the data. Red points were down-weighted in the inversion because of poor coherency.

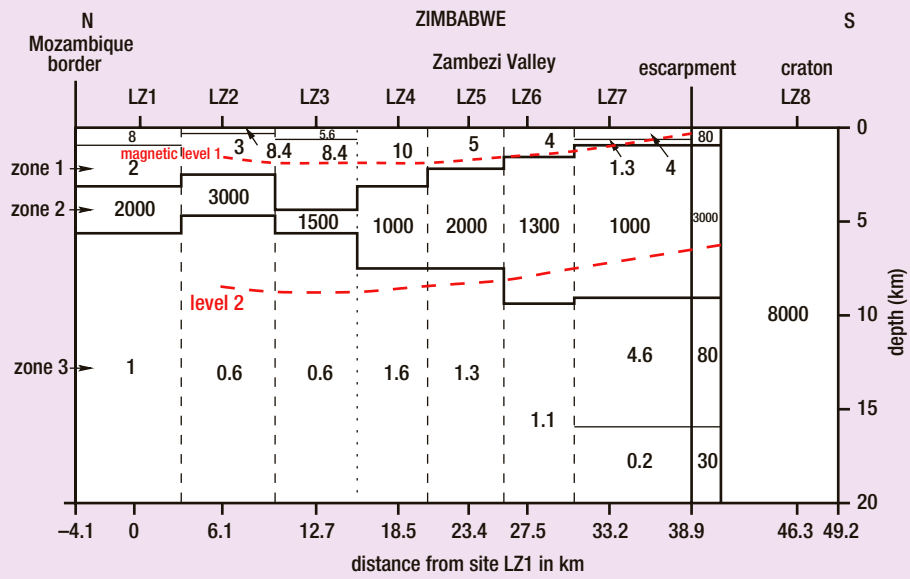

4: The resistivity structure of the Lower Zambezi basin after Losecke *et al.* (1988). Figures indicate resistivity in Ωm. Magnetic levels 1 and 2 indicate the positions of the two horizons deduced from an aeromagnetic survey of the area by Bosum and Geipel (1988).

ial beneath has a resistivity of about 20 Ωm, which is low for basement material, but no localized good conductor similar to that seen elsewhere beneath the Damara orogenic belt is observed. However, this may be because of the data gap at periods between 10 and 100 s, which corresponds to depths around the top of the basement.

A much smaller portion of the adjacent Lower Zambezi basin lies within Zimbabwe, although it is of larger extent. Losecke *et al.* (1988) produced 2-D models of profiles across it from their MT survey; the example in figure 4 is from the profile shown on figure 2. They used a combination of 1-D inversion and 2-D forward modelling, noting the results of the earlier aeromagnetic survey. Their model is divided into three layers of broadly similar resistivity, whose depths and thicknesses vary beneath each site; the model therefore has some lateral smoothness, but this was not a modelling requirement. In this case, there is a very large difference between the apparent resistivities of the two modes within the Zambezi Valley, with the TM mode apparent resistivity curves having a steep negative slope at periods beyond around 2 s and dropping to extremely small values, and the TE mode apparent resistivity levelling out at between 10 and 100 Ωm (see Bailey *et al.* 2000b). The penetration depths of the two modes are thus very different. Losecke *et al.*'s (1988) model is dominated by the TM mode, such that an extremely good conductor (resistivities in the range 0.2–1.6 Ωm) begins at depths of between 5 and 10 km in the valley and continues to the maximum depth extent of the model. The subsequent seismic survey of Hiller and Buttkus (1996) indicates that the lower of the two magnetic horizons inferred by Bosum and Geipel (1988) (figure 4) corresponds to the base of the upper Karoo. Thus the good conductor straddles the seismic basement, indicating that, unlike the situation in the Mana Pools basin, it is a basement feature, as elsewhere along the Damara orogenic belt. Above the good conductor is a resistive (1000–3000 Ωm) wedge, thinning from south to north, with a more conductive surface layer. However, Losecke *et al.*'s (1988) model is a poor fit to the TE mode data, so we investigated alternative models (Bailey 1998, Bailey *et al.* 2000b). Unfortunately, we only had access to the off-diagonal tensor component elements in the geoelectrical strike co-ordinate system determined by Losecke *et al.* (1988), so were unable to undertake tensor decomposition and dimensionality analysis, or estimate distortion effects. There were indications of static shift in the data (such that only phase data were included from one site during inversion). Inverting the two modes separately with RRI gave two very different models (figure 5), with that from the TM mode data having a good conductor similar to Losecke *et al.*'s (1988), and that from the TE mode data reproducing its resistive wedge. However, there are regions of the subsurface that are conductive in the TM mode model and resistive in the TE mode model, indicating the difficulty in fitting the two modes simultaneously. Both models had a much higher resistivity for the Zimbabwe craton than Losecke *et al.*'s (1988); the enormous contrast with the very conductive region in the valley presents numerical difficulties in modelling (the iterative process does not fully converge). For the joint inversion, we included a vertical escarpment fault across which the smoothness constraint was not implemented; the final model (figure 5) fits the TE mode data better overall and is closer in appearance to the model from those data alone. This is quite unusual – the TM mode structure often dominates in joint inversions (Livelybrooks *et al.* 1993). A comparison of the data predictions indicates that the fits of ours and Losecke *et al.*'s (1988) models are similar. Both models have significant discrepancies from the seismic model, and attempts to characterize seismic layers with layers of constant resistivity were unsuccessful (Bailey 1998, Bailey *et al.* 2000b). The lower of

the two magnetic horizons interpreted by Bosum and Geipel (1988) corresponds to the base of the upper Karoo in the seismic model (figures 3 and 4). Losecke *et al.* (1988) interpreted their resistive wedge as a layer of sediments and intercalated sills within the basin. If the intercalations are thin north–south oriented dykes instead, they would be invisible seismically, and give rise to macroscopic resistivity anisotropy, explaining the separation between the two MT modes, which occurs in the phase as well as apparent resistivity (Kellett *et al.* 1992). Alternatively, an oblique contact between the resistive craton and conductive valley preserves their separation over a longer lateral distance than the vertical fault introduced into our RRI model (figure 5) (which is easier to implement numerically) without introducing anisotropy (see figure 17 of Bailey *et al.* 2000b).

More insight into the origin of the conductivity anomalies beneath the Damara orogenic belt has come from a recent high-resolution MT survey in Namibia (Ritter *et al.* 2003). This survey suggests that the conductor there consists of two narrow, subvertical upper to mid-crustal level zones that correlate with the major tectonic boundaries. Ritter *et al.* (2003) interpret the high conductivity in terms of graphite (or other mineralization) enrichment along the shear zones.

Baringo-Bogoria basin, Kenya

The Baringo-Bogoria basin (BBB) lies within the eastern (Kenya) branch of the East African rift. The lakes to the north (Baringo) and south (Bogoria) are currently fresh water and alkaline, respectively, and both have hydrothermal features such as hot springs. In the past, the lakes have been connected, and they have switched between being fresh water and alkaline. Sediment deposition has been controlled by two different structural trends: N–S border faults and NW–SE transverse zones. Alluvial fans have developed adjacent to border faults, and other deposition has been by river channels and in lakes. Several episodes of volcanism have occurred, most extensively in the early/mid-Miocene. The resulting subsurface resistivity pattern was expected to be 3-D, so a 3-D MT survey was carried out, with a station spacing of typically 2 km over the central part of an area of approximately 15 × 25 km. MT data were collected at 24 sites; at these and a further seven sites, DC resistivity soundings were also carried out to determine near-surface structure. The tectonic setting and station distribution are shown in figure 6. This and subsequent figures in this section are reproduced from Hautot *et al.* (2000), which gives more details of all aspects of the project.

The impedance tensor components were derived using the robust remote reference method of Chave and Thomson (1989). Although we

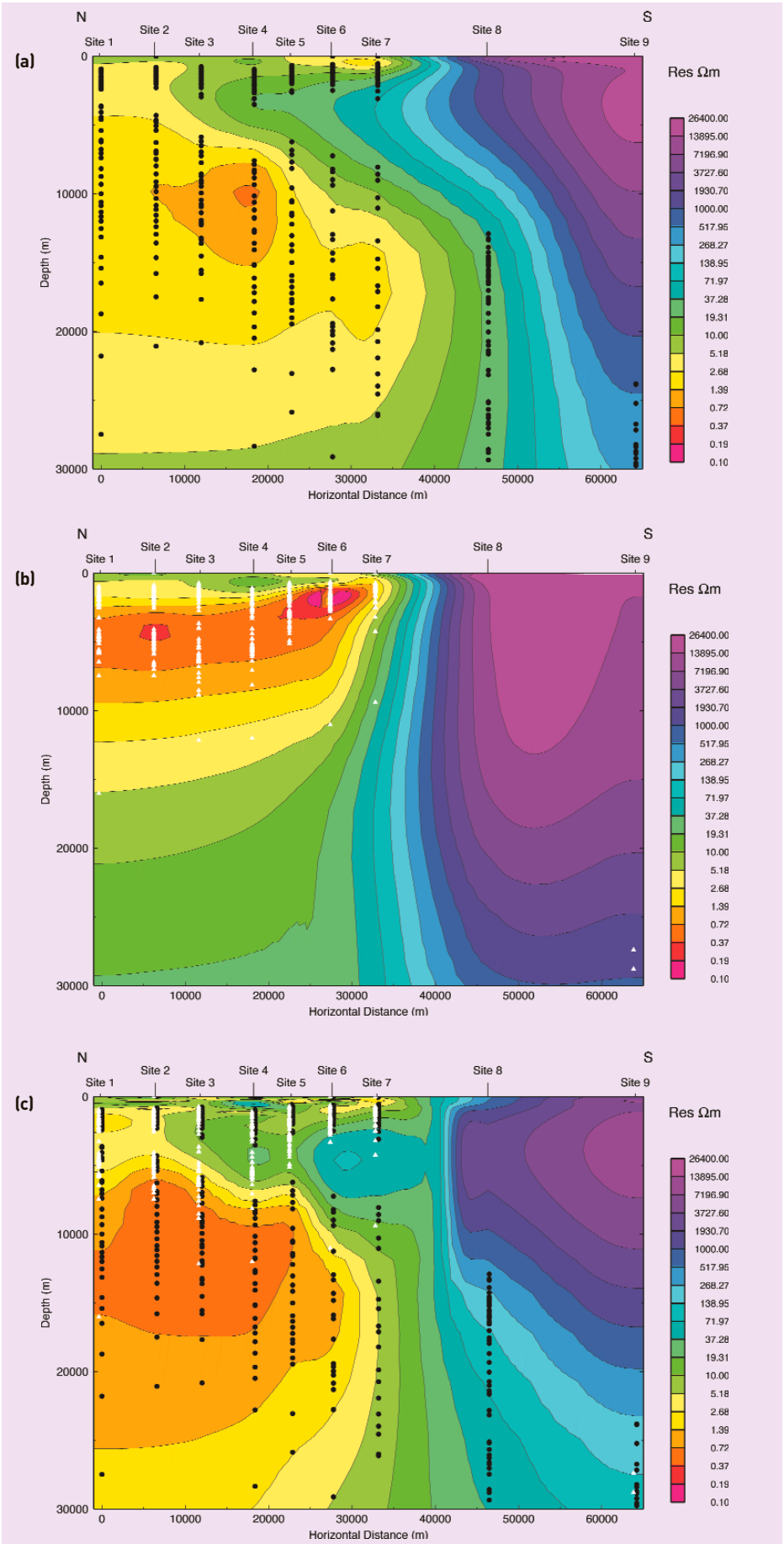

5: The resistivity structure of the Lower Zambezi basin from RRI. (a) From TE polarization data only; (b) from TM polarization data only; (c) from both polarizations simultaneously, with a southern escarpment fault added. Triangles and circles indicate the TM and TE polarization data point skin depths respectively.

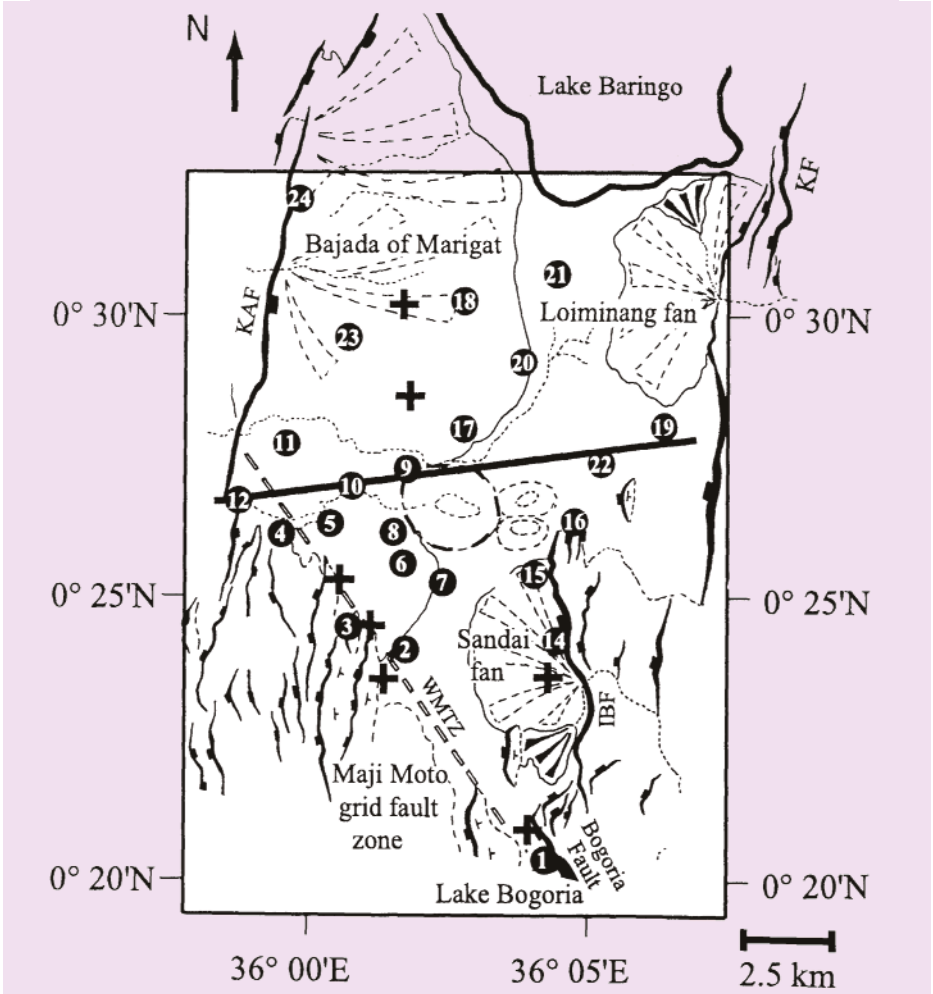

6: Tectonic setting and data distribution of the BBB area of the Kenyan rift. Solid circles are sites where both MT and DC resistivity soundings were undertaken; crosses are sites with just DC resistivity soundings. The box encloses the area of the 3-D model of figure 8. The thick line is the profile along which 2-D RRI gave the starting model for 3-D inversion. WMTZ, Wasages-Marmanet Transverse Zone; KF, Karau Fault; IBF, Ilosowuani-Bechot Fault; KAF, Kapthurin Fault. From Hautot *et al.* (2000).

undertook 3-D modelling, tensor decomposition was carried out using the method of Counil *et al.* (1986), which revealed two dominant trends: N120°–140° at short periods, and N180°–200° at longer periods, corresponding to the transfer zone and main rift axis trends, respectively (figure 6). This also enabled us to derive (using RRI) a representative 2-D model from MT sites along an east–west profile which was used as a starting model for the deeper structure in 3-D inversion, overlying a 3-D resistivity distribution derived from the DC resistivity soundings for the shallow structure. Three-dimensional modelling requires careful parameterization of the region studied, and consideration of the effects of the topography of the rift flanks. The horizontal and vertical grid layout (with resistivity of each block the parameter to be determined) is shown in figure 7. A central 3-D portion of the model volume covers the east–west profile of the 2-D RRI model (16.5 km wide) and extends 25.5 km in the north–south direction; the depth extent was initially 8 km, but increased to 17 km during inversion. The size of the blocks in the horizontal directions is determined by the station distribution; in the vertical direction, they increase with depth. Each block is subdivided into a finer mesh (see figure 7) to improve the accuracy of the forward modelling calculation. The 3-D portion of the model is embedded in a 2-D region to the north and south, in which the model is assumed to have a north–south strike, and a 1-D region to the east and west and below the whole model area. The inversion was carried out in several steps, but allowing all parameters, including those of the 1-D portions of the model space, to vary, until a minimum misfit was obtained, using

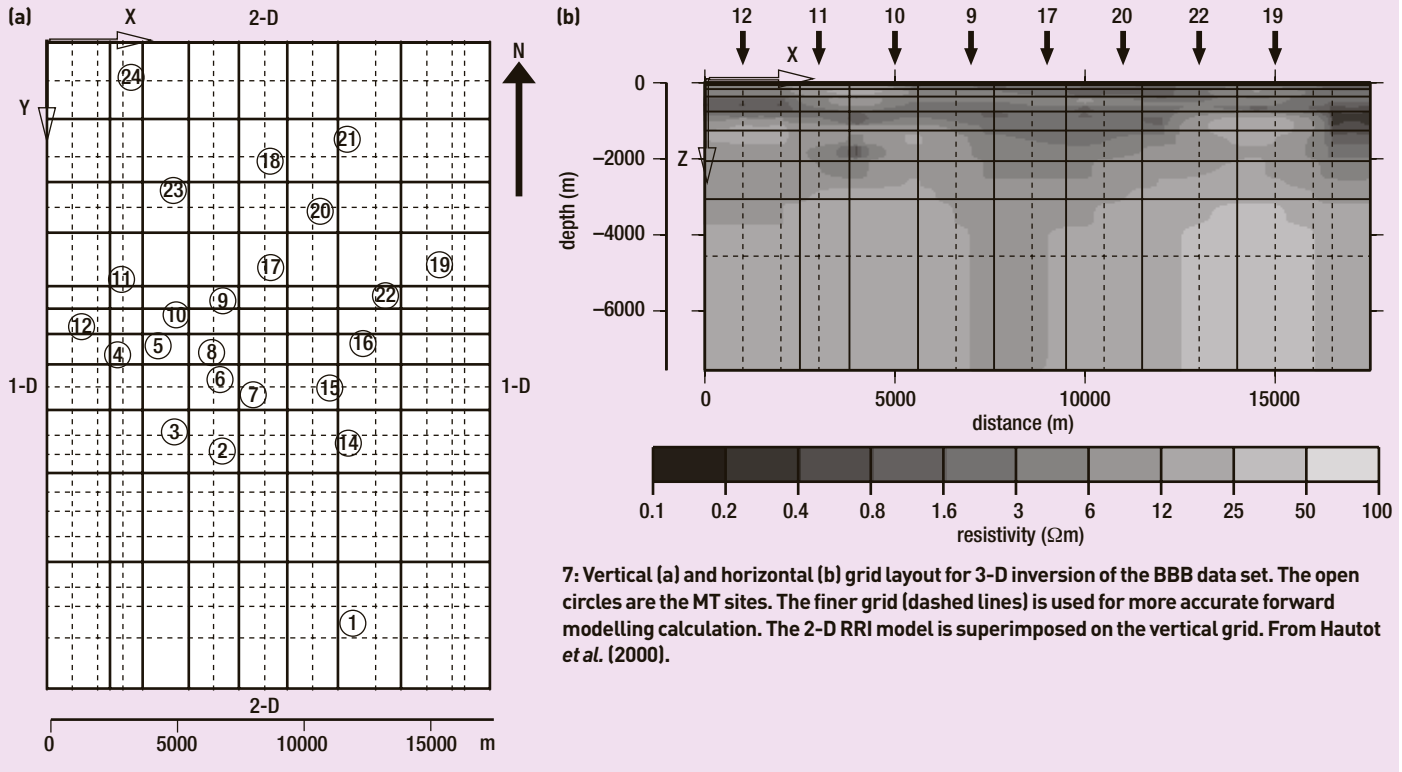

7: Vertical (a) and horizontal (b) grid layout for 3-D inversion of the BBB data set. The open circles are the MT sites. The finer grid (dashed lines) is used for more accurate forward modelling calculation. The 2-D RRI model is superimposed on the vertical grid. From Hautot *et al.* (2000).

a regularization term to control the resistivity contrast between blocks.

The final model, presented in depth slices in figure 8, which is a good fit to the data (see figure 10 of Hautot *et al.* 2000), was subjected to a series of sensitivity tests to establish that the key structures were constrained by the data. This allowed us to propose a new model of rift development in the region. The resistive layer 10 of figure 8, between 1.4 and 4.9 km, was initially thought to be basement, but the conductor beneath (layer 11) suggests it is a thick layer of volcanic rocks underlain by sediments. Thus layer 11 could represent the initial synrift sedimentary infill. Hautot *et al.* (2000) suggest that the volcanic succession is most probably lower to middle Miocene in age, and hence that the proto-Baringo basin would be Palaeogene to lower Miocene, i.e. contemporary with the deep Kerio basin to the west. The structure of layers 8 and 9 is different from that above and below. Here the internal basin structure is dominated by two narrow, north–south oriented conductive structures, labelled Y and Z, and the N140° trending Wasages–Marmanet transverse zone (WMTZ) is only weakly indicated compared with its expression in the layers above. However, layer 7 has a similar structure to the narrow conductor U at the southernmost limit of the model. In layers 6 and 7, the resistivity distribution is dominated by a conductive north–south axis, with resistive features linked to volcanic formations affected by the Kapthurin fault (KAF), Ilosowuani-Bechot fault (IBF) and WMTZ. The north-eastward migration of the WMTZ from its surface position (marked on layer 5) is consistent with a flexural structure. The resistive features surrounding the conductive area labelled X can be correlated with volcanic rocks belonging to the Hannington formation, associated with the fluvio-lacustrine Kapthurin formation (Kfm), and forming the IBF structure. The resistivity contrast along the marked N140° trend following the surface position of the WMTZ may represent the contact between the recent sediments and the Hannington trachyphonolites (HT). Feature X correlates with the present sedimentary basin, and two main axes of deposition can be defined: a north–south one, several kilometres wide in the north and thinning southwards, marking the channels of the main rivers flowing within the rift floor and the Lake Bogoria sedimentary infill, bordered by alluvial fans, and an east–west one, corresponding to lateral sedimentary fluxes from the western and eastern basin borders. The resistivity distribution in layers 1–4 can be related to the Recent sedimentary cover, comprising silts of ~20 m thickness and alluvial fans which have developed on both faulted margins.

The interpretation of this resistivity model suggests a marked modification to previous

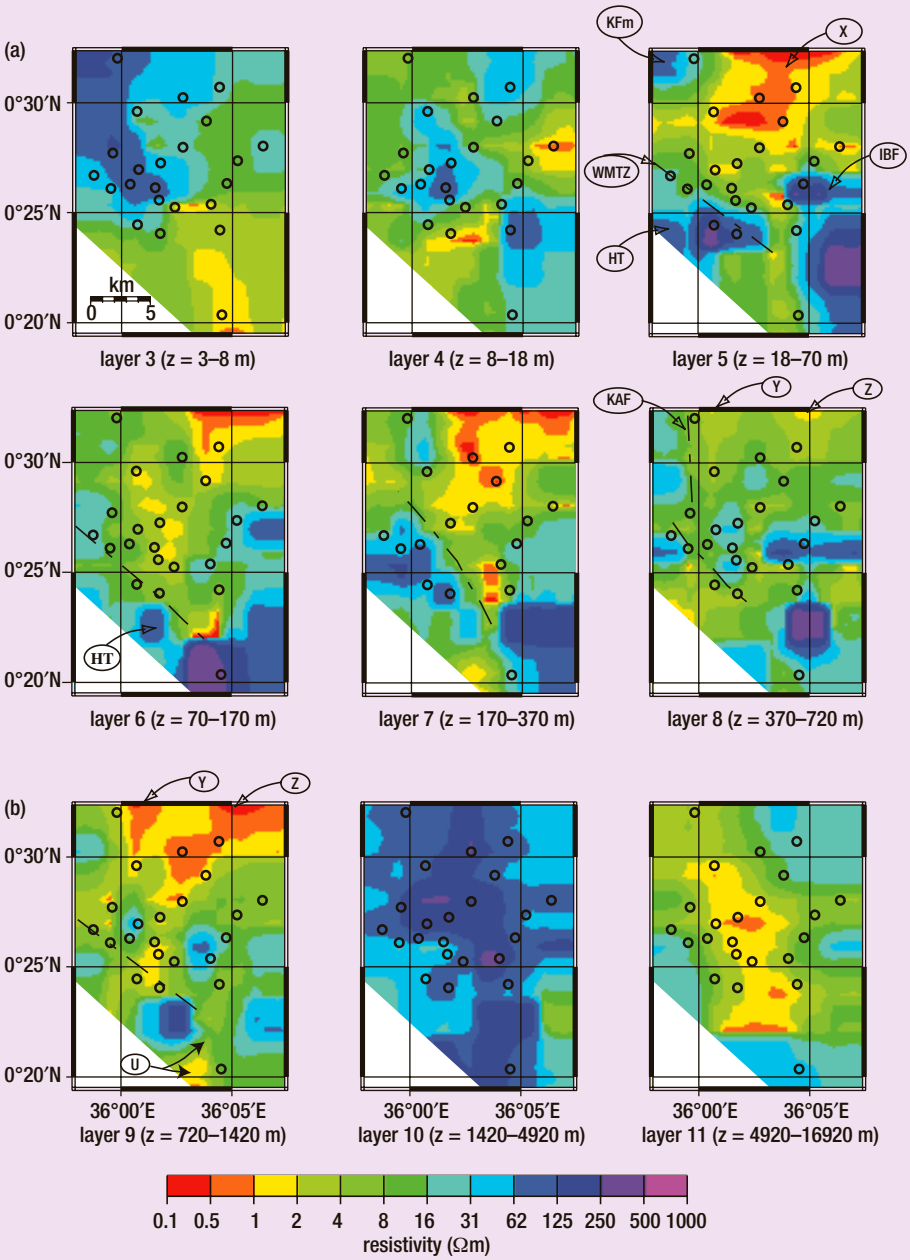

8: Depth slices through the final 3-D model of the BBB, beginning at 3 m below the surface. Open circles indicate the surface positions of the MT sites. The south-west part of the model has been masked because there are no MT sites in the area. See caption to figure 6 for key to most tectonic units. KFm, Kapthurin formation; HT, Hannington Trachyphonolites. Features U, X, Y and Z are described in the text.

models of rift propagation (e.g. Mugisha *et al.* 1997), summarized in figure 13 of Hautot *et al.* (2000). Rifting was believed to have nucleated on the western side of the rift as early as Palaeogene time, with the only expression in the BBB area being moderate flexure in the late Miocene. During Pliocene to Recent time, rift deformation was assumed to have shifted eastwards, focusing along the Baringo-Bogoria zone that belongs to the active axial trough of the Kenyan rift. The existence of a Palaeogene deeply buried basin beneath the Baringo-Bogoria area (layer 11) suggests that the initial rift system was almost twice as wide as previously thought, consisting of two westerly tilted half grabens. The resistivity distribution suggests the initial geometry of the BBB was controlled by both north–south (KAF) and transverse (WMTZ) faults on the successive depocentres. The initial length of the BBB was much greater, with its current rhomb-shaped structure accounted for by subsequent flexure and fault segmentation.

Northern main Ethiopian rift

In 2002/3, a number of geophysical techniques were used in the Ethiopia Afar Geoscientific Lithospheric Experiment (EAGLE) to investigate the transition from continental rifting to sea-floor spreading that is taking place in the northern main Ethiopian rift. These included the deployment of broadband and short-period seismic receivers, the latter along profiles across and

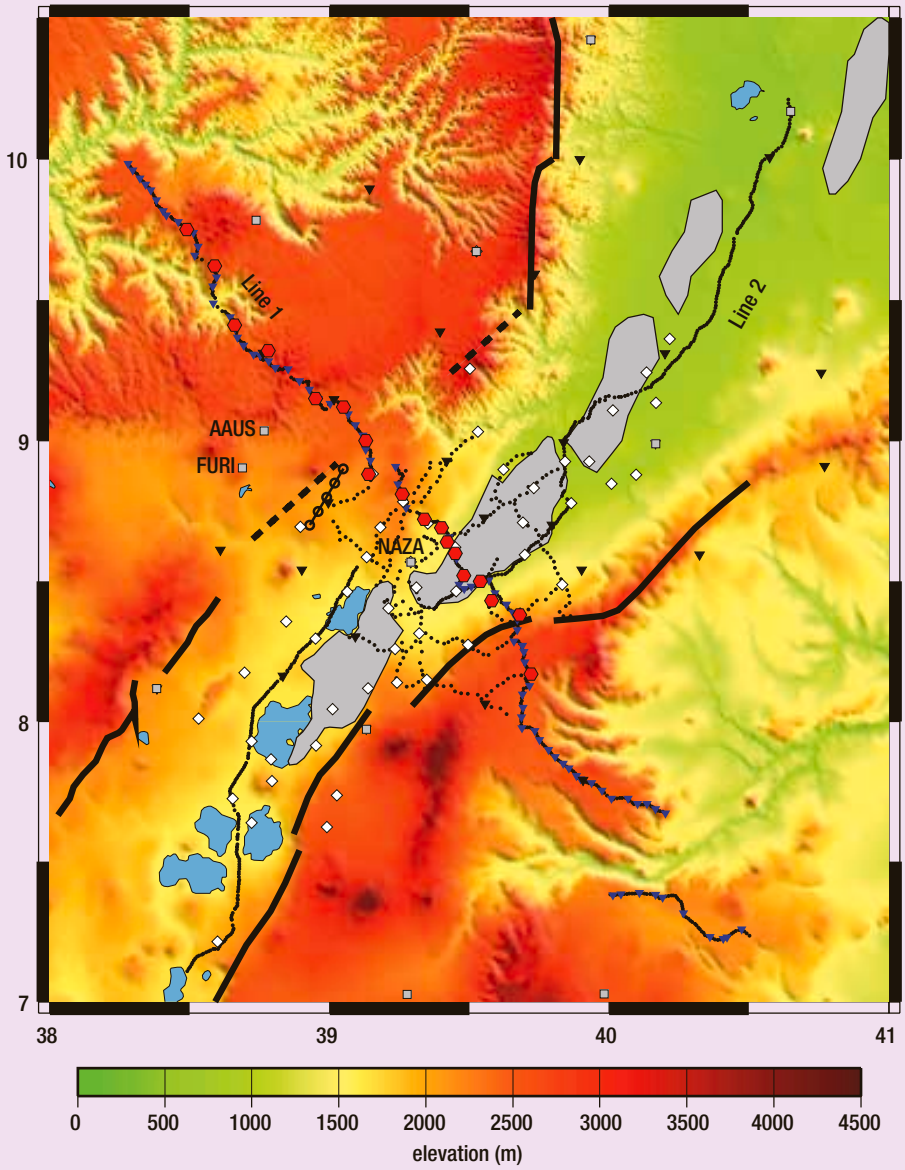

9: MT sites (red hexagons) along the cross-rift (line 1) profile of the EAGLE project, superimposed on the topography, border faults (solid thick black lines), faulted monoclines (dashed thick black lines), Bishoftu Volcanic Chain (linked open circles) and magmatic segments (grey shading) of the northern main Ethiopian rift. Also shown are the seismic stations, both broadband (black inverted triangles and white diamonds, EAGLE phase I and II respectively; blue inverted triangles, EAGLE line 1; grey squares, Pennsylvania State University [Dugda *et al.* 2005]) and short period (black dots, EAGLE along-rift line and central 2-D array). From Whaler and Hautot (2006).

along the rift, and in a 2-D array around their point of intersection, and gravity and MT surveys along the cross-rift profile. The seismic data were used to study seismicity, produce 2-D and tomographic images, investigate crustal thickness and Poisson's ratio from receiver function analysis, and analyse seismic anisotropy from shear wave splitting. The MT sites were located in the same locations as broadband seismic receivers where feasible, to enable a comparison of results. Eighteen MT sites were occupied, at an average spacing of 20 km outside the rift, decreasing to 5 km within it, where higher subsurface conductivities restricting penetration were expected. The station distribution is shown in figure 9. Robust response processing (using the methods of Chave and Thomson 1989 and Ritter *et al.* 2003) showed that one was badly contaminated by cultural noise and was not considered further, but the others all provided usable transfer functions, although some only at shorter periods.

Tensor decomposition using the technique of Counil *et al.* (1986) showed that the data are consistent with 2-D interpretation, with a geoelectric strike direction roughly parallel to the rift border direction (N30°–40°), though turning slightly northwards at sites within the rift. This rotation matches the orientation of the *en echelon* magmatic segments within it (see figure 9) and follows the change in orientation of the shear-wave splitting fast direction (e.g. Kendall *et al.* 2005). Some of the sites suffered from static shift; at the two most badly affected, the near-surface resistivity structure was determined from DC resistivity soundings, and the short-period data this structure predicted was used to remove the static shift. The data were modelled by iterative regularized inversion, and the result is presented in figure 10, taken from Whaler and Hautot (2006) where more details of both the modelling and interpretation can be found.

The shallow conductive near-surface structure of figure 10 reflects the near-surface geology and matches its geometry deduced from surface mapping (Wolfenden *et al.* 2004) and imaged by the cross-rift seismic survey (Mackenzie *et al.* 2005) – Late Miocene-Early Pliocene ignimbrites and rhyolites, and Quaternary sediments and volcanics within the rift, and a few kilometres thickness of pre-rift Jurassic sediments and Oligocene flood basalts beneath, which crop out elsewhere along the profile. The Adama basin appears to have a maximum thickness of 3 km in the MT model, slightly less than inferred from geological mapping and the seismic survey. Beneath the Boset volcano in the rift is an extremely conductive (resistivity 0.8 Ωm) shallow lens which could be caused by a shallow magma zone. There is a good resistivity contrast between the upper and lower crust beneath the northern plateau, at depths matching those inferred seismically, but material beneath the southern plateau is uniformly much more resistive. Figure 10 has two conductive bodies at lower crustal depths, one beneath the Boset magmatic segment and the other close to the rift flanks to the north-west, and slightly deeper. That beneath the segment coincides with a high seismic velocity (Keranen *et al.* 2004) and density (Cornwell *et al.* 2006) body, thought to be caused by ≲1.8 Ma gabbroic mafic intrusion, feeding a series of dykes intruding into the upper crust. The high conductivity would suggest that it is at least partially molten, which makes its high seismic velocity and density even more remarkable. Keir *et al.* (2006) note that seismicity within the rift is confined to the magmatic segment and ceases at a depth of ~10 km. From this they infer that it is caused by dyking into the brittle upper crust, a mechanism that relies on melt still being present. There is no suggestion from other data of a mafic intrusion associated with the second high-conducitvity body to the north-west, but the Bishoftu volcanic chain (BVC on figure 10) to the south-west may be responsible, bearing in mind that the MT method is sensitive to structure some distance away, particularly to conductive features which channel electric current. In fact, there is widespread evidence for partial melt beneath the north-west plateau, including late teleseismic arrivals from all azimuths (i.e. not just from

those arrivals passing through the rift) at the permanent station FURI (figure 9), shear wave splitting inferred to arise from oriented melt pockets, and high Poisson's ratios at a number of nearby sites, though unfortunately not from the sites over the second conductor. The deeper Moho beneath the northern plateau is inferred to be caused by a layer of underplated material of Oligocene and/or Recent age (Mackenzie *et al.* 2005). The two conductors lie within this underplated layer, and may arise from recent low-pressure fractionation involving it partially melting. Two shallow high-resistivity bodies coincide with local peaks in the gravity profile, one of which has been interpreted as a further mafic intrusion (Cornwell *et al.* 2006). Its top surface coincides with the top of the resistor, but it has greater depth extent. Possibly the MT model only images its solidified top, with the warmer, deeper part not having a discernible resistivity contrast with the surroundings.

Joint inversion of the MT and gravity or seismic data sets are planned to explore some of these possible interpretations of the data. Already, the MT data have provided independent evidence for extensive partial melt beneath both the rift and the northern plateau, and a difference in crustal structure between the northern and southern plateaux. The rotation in geoelectric stike direction within the rift supports the magma-assisted rifting hypothesis of Ebinger and Casey (2001) and Buck (2004), whereby the border faults have been abandoned and strain is now taken up within the magmatic segments in the transition from continental rifting to sea-floor spreading. ●

K A Whaler, Institute of Earth Science, School of GeoSciences, University of Edinburgh, UK; kathy.whaler@ed.ac.uk.

Acknowledgments. Many people have collaborated with me or otherwise contributed to the success of the projects outlined above, through help with the logistics, fieldwork, equipment, data processing, modelling and interpretation. These include, but are no means confined to, Laike Asfaw, Atalay Ayele, David Bailey, Ian Bastow, Johan de Beer, Colin Brown, Dave Cornwell, Graham Dawes, Mohammednur Desissa, Cindy Ebinger, Oswald Gwavava, Volker Haak, Sophie Hautot, Abiy Hunegnaw, Phil Jones, Derek Keir, Mike Kendall, Graeme Mackenzie, Peter Maguire, Oliver Ritter, Graham Stuart, the late Samson Takaedza, Pascal Tarits, Jean-Jacques Tiercelin, Ute Weckmann, Teddy Zengeni and the EAGLE Working Group. In addition, funding has come from the NERC through the Geophysical Equipment Facility, a PhD studentship to David Bailey and several research grants, and an EU (Marie Curie) Fellowship to Sophie Hautot. The British Council, Elf Petroleum Norge AS, the National Oil Corporation of Kenya, the Ministry of Mines and Energy of Ethiopia, and the universities of Addis Ababa and Zimbabwe have also provided funding or assistance in kind.

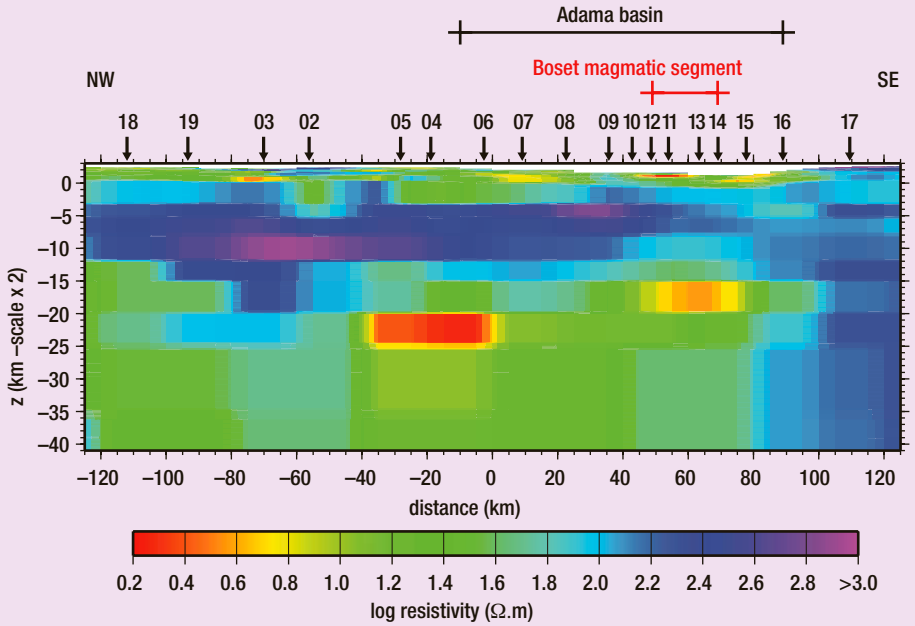

10: 2-D model of the resistivity structure across the main Ethiopian rift, from an inversion of both the TE and TM mode data on a finite difference grid. Station numbers, the extent of the Boset magmatic segment and Adama basin, and the projection of the Bishoftu Volcanic Chain (BVC) onto the model, are indicated along the top. The Adama basin terminates to the south-east against the Arboye rift border fault (Wolfenden *et al.* 2004). Data from site 12 were not included in the inversion because they were too badly contaminated by cultural noise. From Whaler and Hautot (2006).

References

Bahr K 1988 *J. Geophys.* **62** 119–127.
Bahr K 1991 *Phys. Earth Planet. Interiors* **66** 24–38.
Bailey D S 1998 Magnetotelluric studies of the Zambezi mobile belt of Northern Zimbabwe, PhD thesis, University of Edinburgh.
Bailey D *et al.* 2000a *J. Geophys. Res.* **105** 11 185–11 202.
Bailey D *et al.* 2000b *Geophys. J. Int.* **142** 898–914.
Balasis G *et al.* 1997 *Geophys. J. Int.* **129** 472–473.
Bosum W and Geipel H 1988 *Reinterpretation of an aeromagnetic profile in the Zambezi Valley of Zimbabwe on the basis of magnetotelluric and gravimetric data* technical report (Bundesanstalt Für Geowissenschaften und Rohstoffe, Hanover).
Brewitt-Taylor C R and Weaver J T 1976 *GJRAS* **47** 375–396.
Buck W R 2004 in Karner G D *et al.* (eds) *Rheology and deformation of the lithosphere at continental margins* (Columbia Univ. Press, New York) 1–30.
Chave A D and Thompson D J 1989 *J. Geophys. Res.* **94** 14 202–14 215.
Constable *et al.* 1987 *Geophysics* **52** 289–300.
Cornwell D G *et al.* 2006 in Yirgu G *et al.* (eds) *Structure and Evolution of the East African Rift System in the Afar volcanic province* Geol. Soc. London Spec. Pub. **259** 309–323.
Counil J–L *et al.* 1986 *Ann. Geophys.* **4** 115–130.
deGroot-Hedlin C and Constable S 1990 *Geophysics* **55** 1613–1624.
Dugda M T *et al.* 2005 *J. Geophys. Res.* **110** doi 10.1029/2004JB003065.
Ebinger C and Casey M 2001 *Geology* **29** 527–530.
Egbert G D and Booker J R 1986 *Geophys. J. R. astr. Soc.* **87** 173–194.
Gamble T D *et al.* 1979 *Geophysics* **44** 53–68.
Groom R W and Bailey R C 1989 *J. Geophys. Res.* **94** 1913–1925.
Haak V and Hutton R 1986 in J B Dawson *et al.* (eds) The Nature of the Lower Continental Crust *Geol. Soc. London Spec. Pub.* **24** 35–49.
Hautot S *et al.* 2000 *J. Geophys. Res.* **105** 23 493–23 518.
Hiller K and Buttkus B 1996 *Z. angew. Geol.* **42** 132–137.
Keir D *et al.* 2006 *J. Geophys. Res.* in press.
Kellett R L *et al.* 1992 *Geophys. J. Int.* **111** 141–150.
Kendall J-M *et al.* 2005 *Nature* **433** 146–148.
Keranen K *et al.* 2004 *Geology* **32** 949–952.
Livelybrooks D *et al.* 1993 *Phys. Earth Planet. Interiors* **81** 67–84.
Losecke W *et al.* 1988 *Technical Report* 84.2171.1 (Bundesanstalt für Geowissenschaften und Rohstoffe, Hanover).
Mackenzie G D *et al.* 2005 *Geophys. J. Int.* **162** 994–1006.
Meju M A 1996 *Geophysics* **61** 56–65.
Mugisha F *et al.* 1997 *Tectonophys.* **278** 61–81.
Orpen J L *et al.* 1989 *J. Afr. Earth Sci.* **8** 215–229.
Parker R L 1980 *J. Geophys. Res.* **85** 4421–4428.
Parker R L and Booker J R 1996 *Phys. Earth Planet. Interiors* **98** 269–282.
Pek J and Verner T 1997 *Geophys. J. Int.* **128** 505–521.
Ritter O *et al.* 1998. *Geophys. J. Int.* **132** 535–548.
Ritter O *et al.* 2003 *Phys. Earth. Planet. Int.* **138** 71–90.
Simpson F and Bahr K 2005 *Practical magnetotellurics* (Cambridge University Press, Cambridge).
Smith J T 1995 *Geophys. J. Int.* **122** 219–226.
Smith J T and Booker J R 1991 *J. Geophys. Res.* **96** 3905–3922.
Swift C M 1967 in Vozoff K (ed.) Magnetotelluric Methods *Society of Exploration Geophysicists, Geophysics Reprints* **5** 156–166.
Telford W M *et al.* 1990 *Applied Geophysics* (Cambridge University Press).
Vozoff K 1972 *Geophysics* **37** 98–141.
Wannamaker P E *et al.* 1987 *Geophys. J. Roy. Astr. Soc.* **88** 277–296.
Whaler K A and Hautot S 2006 in Yirgu G *et al.* (eds) The Structure and Evolution of the East African Rift System in the Afar Volcanic Province *Geol. Soc., London, Spec. Pub.* **259** 295–307.
Wolfenden E *et al.* 2004 *Earth Planet. Sci. Letts.* **224** 213–228.
Zhang P *et al.* 1987 *Geophysics* **52** 267–278.